Computational Fluid Dynamics Modelling of Slurry Transport by Pipeline

***Mingzhi Li[1], †Yanping He[1,2,3] , Yadong Liu[1,2,3], Chao Huang[1,2,3]**

[1] School of Naval Architecture, Ocean & Civil Engineering, Shanghai Jiao Tong University, Shanghai 200240, China
[2] State Key Laboratory of Ocean Engineering, Shanghai Jiao Tong University, Shanghai 200240, China
[3] Collaborative Innovation Center for Advanced Ship and Deep-Sea Exploration (CISSE), Shanghai 200240, China

*Presenting author: limz_2008@sjtu.edu.cn
†Corresponding author: hyp110@sjtu.edu.cn

The flow velocity and solid concentration distributions of solid–liquid (slurry) flows transported by pipeline are investigated using a steady three-dimensional (3D) hydrodynamic model based on the kinetic theory of granular flow. Slurries of varying solid particle concentration, grain diameter, and flow conditions are studied, and the effects of particle–particle and particle–wall collisions and near-wall lift force on the concentration distribution are modelled. The simulation agrees well with various experimental results in the literature. The simulation shows that the solid concentration distribution is asymmetric in the vertical plane, and its degree of asymmetry increases as the solid concentration decreases, the mixture velocity decreases, the particle size increases, or the pipe diameter increases. The solid concentration decreases rapidly near the pipe wall due to collisions with the wall. Fine particles smaller than the thickness of the viscous sublayer are most concentrated near the pipe bottom (maximum concentration at the relative location $y_{max}/D \approx 0.02D$, where D is the pipe diameter) in the viscous sublayer, while the greatest concentration of coarser particles is away from the pipe bottom ($y_{max}/D \approx 0.1D$), outside of the viscous sublayer. The solid velocity distribution is also asymmetric: maximum-velocity points deviate from the pipe centre, and increasing the solid concentration gradually shifts the point of maximum velocity downward. These results lay a solid foundation for further study of the resistance mechanism and pipe wear, and can be used as a reference for analysing the mesoscopic processes of slurry transport by pipeline.

Keywords: Eulerian multiphase model; Concentration distribution; Particle kinetic; Slurry transport; Pipeline; Dredging; Deep-sea mining

1. Introduction

In recent decades, pipelines have been promoted for the transport of various solids (as slurry mixtures) owing to their insulation from the environment and ability to run uninterrupted, thus reducing the required investment and operating costs. Pipelines can achieve high efficiency, low energy use, environmental protection, and ease of implementation and control. They have been widely applied in many fields such as coal, metallurgy, and mining. Pipelines used for dredging alone have contributed hundreds of billions of US dollars to the global economy in recent years. Pipelines have also been considered as potentially useful in emerging technologies such as ocean mining.

Most research about slurry pipeline transport has focused on predicting friction loss and critical velocity (i.e., no stable particle bed, the lowest pressure loss point), but recently more attention has been paid to the operational costs arising from pipeline wear and maintenance. Industrially transported slurry is generally heterogeneous within the pipeline because the lower half has a greater solid concentration than the upper half (due to gravity), and will thus suffer worse wear. The safety and lifetime of a pipeline can be improved by rotating according to the degree of abrasion around the circumference. This requires accurate prediction of pipeline wear around the circumference, and a proper model for predicting the slurry concentration and velocity distributions is the precondition.

Existing models of slurry pipeline transport can predict with varying degrees of accuracy parameters such as pressure drop, particle settling velocity, and solid concentration distribution under different working conditions, given data regarding the pipe diameter, particle size, slurry concentration, etc. However, most are empirical formulae, based on dimensionless parameters such as excess pressure, Froude number, and solid concentration derived from experimental data, or are semi-empirical formulae based on the theories of gravity, energy, etc. It is impossible theoretically to characterize, for example, the turbulence intensity or particle momentum exchange in a pipeline, but these microscopic characteristics often greatly affect the pipeline characteristics in practice with varying in-situ gradations and operating conditions. Understanding the variability of these parameters in different positions within a pipeline is critical to the proper modelling of factors such as pipe wear, energy loss, and slurry flow regime in practice.

Existing models cannot accurately predict the particle concentration distribution near the bottom of the pipe, especially when the maximum concentration of coarse particles is located away from the bottom (Kaushal and Tomita, 2007). However, the solid concentration distribution near the wall determines the local solid pressure, wall shear stress, and friction resistance, and thus has a critical effect on pipeline wear. Therefore, accurate prediction of the solid concentration distribution, especially near the pipeline wall, is the key not only to predicting wear but also to calculating friction resistance. The solid concentration and velocity distribution (and their variation in a pipe under different conditions) are important to understanding the mechanism of pressure drop and predicting the degree of wear in a pipeline. They can also help improve economic efficiency.

Developments of computer technology and calculation methods have allowed computational fluid dynamics (CFD) to be widely applied in engineering. While CFD has yet to develop full models of solid–liquid two-phase flow (most models refer to gas–liquid two-phase flow theory), simulations of velocity distribution and solid concentration distribution are relatively mature. Current CFD technology includes 3D horizontal pipeline CFD models based on granular kinetic theory, which have been established for comparison with published experimental results and to study the effects on velocity distribution and concentration distribution of the particle concentration, particle size, slurry velocity, and pipe diameter. Before discussing the calculation method and results, a brief view of current work in this field is presented.

2. Previous Work

While the study of slurry pipeline transport has shown continual progress, research has tended to focus on pressure drop and critical velocity. For example, the established Durand (1952)

formula, based on experimental data, is favoured by much of the European dredging industry. The Wilson and Addie (1997) formula is widely used by American dredgers. Wasp et al.'s (1977) two-phase flow model considers particle concentration distribution during transport. Turian and Yuan (1977) developed a formula that can fit different dimensionless parameters to experiment data. Doron and Barnea's (1993) formula for a three-layer model is based on mechanical balance, and Lahiri and Ghanta's (2008) formula fits existing experimental data by means of genetic algorithm. The Delft head loss and limit deposit velocity framework (DHLLDV) reported by Miedema and Ramsdell (2015a) probes the mechanism of pressure drop, and developed an applicable and convenient system by using parameters that are easily obtained. Theoretical analysis has improved from the earliest empirical formulae based on purely dimensionless analysis to lift force theory, energy theory, and two-phase flow theory; however, microscopic parameters such as turbulent dissipation force, particle collision force, and particle momentum exchange are not yet properly modelled.

Many scholars have made significant contributions to the study of concentration distributions, including Karabelas (1977), Roco and Shook (1983), Kaushal and Tomita (2002, 2007), Kaushal et al. (2005), and Gillies *et al*. (2004). Their various experimental studies have considered variables such as pipe diameter, particle size, and flow conditions. Miedema (2017) and others have published methods to calculate vertical solid-concentration profiles in pipelines given previous experimental data for flow parameters such as eddy diffusivity and particle settling velocity. Each formula can represent the concentration distribution with varying degrees of accuracy, but they rely less on flow parameters than empirical coefficients, thus limiting their applicability and accuracy to the quality of the experimental data and the experience of the user. Experiments by Kaushal and Tomita (2007) for specific particle sizes (diameters of 0.125 and 0.44 mm) found maximum concentrations of coarse particles in the zone away from the wall at about 0.2 D rather than at the bottom of the pipe. This result supported the speculation of Wilson and Sellgren (2003) about the effect of near-wall lift on the particle concentration near the bottom of the pipe, but no mathematical model has yet predicted and interpreted this finding (Kaushal *et al*., 2012).

Numerical simulations include Ling et al.'s (2003) simulation of low-density slurry flows in a fully developed turbulent model using the algebraic slip mixture (ASM) in ANSYS Fluent; the results agree well with experimental data. Kaushal *et al.* (2012) carried out numerical simulations of mono-dispersed fine particles at high concentration using the Eulerian model and mixture model in ANSYS Fluent (0.125 mm diameter glass beads in a 54.9 mm pipe); comparison with experimental results showed the Eulerian model to give more accurate predictions for both the pressure drop and concentration profile than the mixture model. However, the model results differed slightly from Kaushal and Tomita's (2007) experimental data, especially near the bottom of the pipeline. Ekambara *et al.* (2009) predicted horizontal solid–liquid pipeline flows under a wide range of conditions using the two-fluid model in ANSYS-CFX, and simulated results close to observed data. Messa *et al.* (2014, 2015) developed a two-fluid model and used it in PHOENICS software to simulate fully suspended liquid–solid slurry flows in horizontal pipes. The model considered turbulent dissipation, momentum exchange, and the influence of wall shear stress on grains, and it provided a method of wall function calculation with improved computing speed and accuracy. No previous models can accurately calculate the particle concentration distribution near the wall, especially for

coarse particles, or calculate the effect of the wall lift force.

In addition, the existing formula for horizontal pipes, although it can predict slurry characteristics under various operating conditions such as friction resistance and solid concentration, cannot be applied to complex geometric spaces such as loop lines and gate valves owing to its empirical nature not taking into account factors such as slurry turbulence, particles collisions, and energy exchange. This limits its applicability in practice, because the pipeline systems for dredging, mining, and coal inevitably include pumps, angular pipes, pipe branches, and other complex spaces. The model will thus fail to understand the properties of the entire system. Therefore, to develop a universal model is an important research goal.

To overcome the above limitations, an integrated model is developed using ANSYS Fluent, based on granular kinetic theory. This model can accurately describe the dynamic characteristics of slurry transport by pipeline.

3. Mathematical Modelling

The Eulerian multiphase model is used here. It mathematically treats the different phases as interpenetrating continua. Granular kinetic theory is used to describe interactions between the particles. A single pressure is shared by all phases. The conservation equations of mass, momentum, and energy are solved individually for each of the phases. Coupling of all phases is then achieved by pressure and interphase exchange coefficients. The model considers energy dissipation and energy exchange caused by particles. Interfacial forces such as the drag force caused by speed differences between phases, the virtual mass force by particle acceleration, the lift force by phase velocity gradient, and other forces are also considered. The Eulerian multiphase model is suitable for simulating slurry transport in pipelines over a wide range of operating conditions.

3.1 Conservation of Mass

Multiphase flow is modelled as a primary phase and n secondary phases. The primary phase is designed as water, and each secondary phase presents particles of different size ranges, which may or may not be of equal volume fraction. These volume fractions, including that for water, are assumed to be continuous in space and time, and their sum is equal to one.

$$\sum_{q=1}^{n+1} \alpha_q = 1 \tag{1}$$

For multiphase flows, each phase volume fraction is less than its maximum allowed value. Therefore, each phase in the model is considered a compressible fluid satisfying the Eulerian continuity equation.

$$\frac{1}{\rho_{rq}}\left[\frac{\partial}{\partial \mathrm{t}}(\alpha_q \rho_q) + \nabla \cdot (\alpha_q \rho_q \vec{v}_q) = \sum_{p=1}^{n}\left(\dot{m}_{pq} - \dot{m}_{qp}\right)\right] \tag{2}$$

where ρ_{rq} is the q^{th} phase reference density, or the volume averaged density of the q^{th} phase in the solution domain, α_q is the volume fraction of phase q, $\vec{v}_q$ is the velocity of phase q, and $\dot{m}_{pq}$ characterizes the mass transfer from the p^{th} to q^{th} phase. All these mechanisms can be specified separately.

3.2 Conservation of Momentum

Each phase q in the Eulerian multiphase model must conserve momentum via the following equation:

$$\frac{\partial}{\partial t}(\alpha_q \rho_q \vec{v}_q) + \nabla \cdot (\alpha_q \rho_q \vec{v}_q \vec{v}_q) = -\alpha_q \nabla p - \nabla p_q + \nabla \bullet \bar{\bar{\tau}}_q + \alpha_q \rho_q \vec{g} + \sum_{p=1}^{n} \left(\vec{R}_{pq} + \dot{m}_{pq} \vec{v}_{pq} - \dot{m}_{qp} \vec{v}_{qp} \right) + \vec{F}_q \quad (3)$$

where p is the pressure, which is equal for each phase at any given point; p_q is the q^{th} phase solid pressure, which is equal 0 for any liquid phase; g is acceleration due to gravity; $\vec{R}_{pq}$ is the interphase force; $\vec{v}_{pq}$ is the interphase velocity; n is the total number of phases; and $\vec{F}_q$ is the sum of the external forces (such as lift force, virtual mass force, wall lubrication force and turbulent dispersion force); $\bar{\bar{\tau}}_q$ is the q^{th} phase stress–stain tensor.

3.3 Conservation of Energy

The first law of thermodynamics is applied in ANSYS Fluent to solve the conservation of energy:

$$\frac{\partial}{\partial t}(\alpha_q \rho_q h_q) + \nabla \cdot (\alpha_q \rho_q \vec{u}_q h_q) = \alpha_q \frac{dp_q}{dt} + \bar{\bar{\tau}}_q : \nabla \vec{u}_q - \nabla \vec{q}_q + S_q + \sum_{p=1}^{n} \left(Q_{pq} + \dot{m}_{pq} h_{pq} - \dot{m}_{qp} h_{qp} \right) \quad (4)$$

where h_q is the specific enthalpy of the q^{th} phase, $\vec{q}_q$ is the heat flux, S_q is a source term that includes sources of enthalpy, Q_{qp} is the intensity of heat exchange between the q^{th} and p^{th} phases, and h_{qp} is the interphase enthalpy. The heat exchange between phases must comply with the local balance conditions $Q_{qp} = -Q_{pq}$ and $Q_{pp} = Q_{qq} = 0$.

3.4 Solids Pressure

For granular flows, the solids pressure is determined by the intensity of the particle collisions and velocity fluctuations. This work calculates the solids pressure using the model of Lun *et al*. (1984):

$$p_q = \alpha_q \rho_q \Theta_q + \sum_{p=1}^{n} 2 \frac{d_{pq}^3}{d_q^3} \left(1 + e_{qp}\right) g_{0,pq} \alpha_p \alpha_q \rho_q \Theta_q \quad (5)$$

The particle pressure consists of a kinetic term corresponding to the momentum transport caused by particle velocity fluctuations and a second term related to particle collisions.

Granular temperature, Θ_q, is solved by the transport equation derived from kinetic theory.

3.5 Transport Equation

The Eulerian multiphase flow model uses a multi-fluid granular model to describe the flow behaviour of a fluid–solid mixture. Solid-phase stresses are key elements derived by making an analogy between the random particle motion arising from particles' inelastic collisions with each other and the walls. The stresses are defined as a function of granular temperature representing the particle velocity fluctuations proportional to the mean square of the random motion of particles. The granular temperature is solved by the transport equation in the model, as follows:

$$\frac{3}{2}\left[\frac{\partial}{\partial t}(\alpha_q \rho_q \Theta_q) + \nabla \cdot (\alpha_q \rho_q \vec{v}_q \Theta_q)\right] = \left(-p_q \bar{\bar{I}} + \bar{\bar{\tau}}_q\right) : \nabla \vec{v}_q + \nabla \cdot (k_{\Theta q} \nabla \Theta_q) - \gamma_{\Theta q} + \varphi_{pq} \quad (6)$$

The left-hand side of the equation represents the net change in fluctuating energy. The first term, $\left(-p_q \bar{\bar{I}} + \bar{\bar{\tau}}_q\right) : \nabla \vec{v}_q$, on the right-hand side represents the generation of energy by the solid stress tensor. The second term, $\nabla \cdot (k_{\Theta q} \nabla \Theta_q)$ is the diffusion of energy in the solid phase. The third term, $\gamma_{\Theta q}$, is the collisional dissipation of energy, and φ_{pq} is the exchange of fluctuating energy between the liquid and the solid phase.

The term $k_{\Theta q}$ is the diffusion coefficient given by Gidaspow *et al*. (1992) as an optional model in ANSYS Fluent:

$$k_{\Theta q}=\frac{150\rho_q d_q\sqrt{\Theta_q\pi}}{384\left(1+e_q\right)g_{0,q}}\left[1+\frac{6}{5}\alpha_q g_{0,q}\left(1+e_q\right)\right]^2+2\rho_q\alpha_q^2 d_q\left(1+e_q\right)g_{0,q}\sqrt{\frac{\Theta_q}{\pi}} \tag{7}$$

where $\gamma_{\Theta q}$ is the rate of energy dissipation within the q^{th} solid phase due to collisions between particles. Lun *et al*. (1984) give $\gamma_{\Theta q}$ as an optional model:

$$\gamma_{\Theta q}=\frac{12\left(1+e_q^2\right)g_{0,q}}{d_q\sqrt{\pi}}\rho_q\alpha_q^2\Theta_q^{1,5} \tag{8}$$

Although equation (6) can be solved for the granular temperature, the procedure is complex and convergence is difficult. ANSYS Fluent by default uses a simpler and computationally more efficient model called "algebraic formulation" that neglects convection and diffusion in the transport equation.

3.6 Turbulence Equations

The per-phase turbulence model is used here. It includes a set of *k*-*ε* transport equations for each phase:

$$\begin{aligned}\frac{\partial\left(\alpha_q\rho_q k_q\right)}{\partial t}+\nabla\cdot\left(\alpha_q\rho_q\vec{U}_q k_q\right)&=\nabla\cdot\left(\alpha_q\left(\mu_q+\frac{u_{t,q}}{\sigma_k}\right)\nabla k_q\right)+\left(\alpha_q G_{k,q}-\alpha_q\rho_q\varepsilon_q\right)\\&+\sum_{p=1}^{n}K_{pq}\left(C_{pq}k_p-C_{qp}k_q\right)-\sum_{p=1}^{n}K_{pq}\left(\vec{U}_p-\vec{U}_q\right)\frac{u_{t,p}}{\alpha_p\sigma_p}\nabla\alpha_p\\&+\sum_{p=1}^{n}K_{pq}\left(\vec{U}_p-\vec{U}_q\right)\frac{u_{t,q}}{\alpha_q\sigma_q}\nabla\alpha_q+\Pi_{kq}\end{aligned} \tag{9}$$

and

$$\begin{aligned}\frac{\partial\left(\alpha_q\rho_q\varepsilon_q\right)}{\partial t}+\nabla\cdot\left(\alpha_q\rho_q\vec{U}_q\varepsilon_q\right)&=\nabla\cdot\left(\alpha_q\left(\mu_q+\frac{u_{t,q}}{\sigma_\varepsilon}\right)\nabla\varepsilon_q\right)+\frac{\varepsilon_q}{k_q}\left(C_{1\varepsilon}G_{k,q}-C_{2\varepsilon}\rho_q\varepsilon_q\right)\\&+C_{3\varepsilon}\frac{\varepsilon_q}{k_q}\left[\sum_{p=1}^{n}K_{pq}\left(C_{pq}k_p-C_{qp}k_q\right)-\sum_{p=1}^{n}K_{pq}\left(\vec{U}_p-\vec{U}_q\right)\frac{u_{t,p}}{\alpha_p\sigma_p}\nabla\alpha_p\right]\\&+C_{3\varepsilon}\frac{\varepsilon_q}{k_q}\sum_{p=1}^{n}K_{pq}\left(\vec{U}_p-\vec{U}_q\right)\frac{u_{t,q}}{\alpha_q\sigma_q}\nabla\alpha_q+\Pi_{\varepsilon q}\end{aligned} \tag{10}$$

where $C_{1\varepsilon}$ is the C1-epsilon number, $C_{2\varepsilon}$ is the C2-epsilon number, $C_{3\varepsilon}$ is the C3-epsilon number, σ_k is the TKE Prandtl number, and σ_ε is the TKR Prandtl number. Their default values are 1.44, 1.92, 1.3, 1.0, and 1.3, respectively.

4. Simulation Method

4.1 Physical Model

To ensure the model's adaptability and universal applicability, a large range of pipe diameters, particle sizes, and solid concentrations are considered here. To allow comparison with experimental data, the horizontal pipes are modelled with inner diameters, D, of 51.5, 54.9, 103, 206, and 495 mm; in each case the length, $L \approx 60D$. To ensure the computations are of good quality and able to converge, 30 boundary layers are established along the surface with a growth factor of 1.2 (i.e., each row of the boundary layer mesh is 20% thicker than the previous one), and the outermost layer has a height of about 0.08 mm. The first layer height from the wall of these models, expressed as a dimensionless parameter y+, is y+ < 30, and reaches y+ < 15. These 3D models include around 10 million meshes, as shown in figure 1.

The following physical properties are employed: for the liquid phase, density

ρ_l = 998.2 kg/m^3 and dynamic viscosity μ_l = 1.003 × 10^{-3} Pa·s, and for the solid phase, particle density ρ_s = 2470–2650 kg/m^3, particle diameter d_p = 0.09, 0.125, 0.165, 0.27, and 0.44 mm, the limiting volume concentration is 0.6–0.7, and the default value of the internal friction angle is 30°.

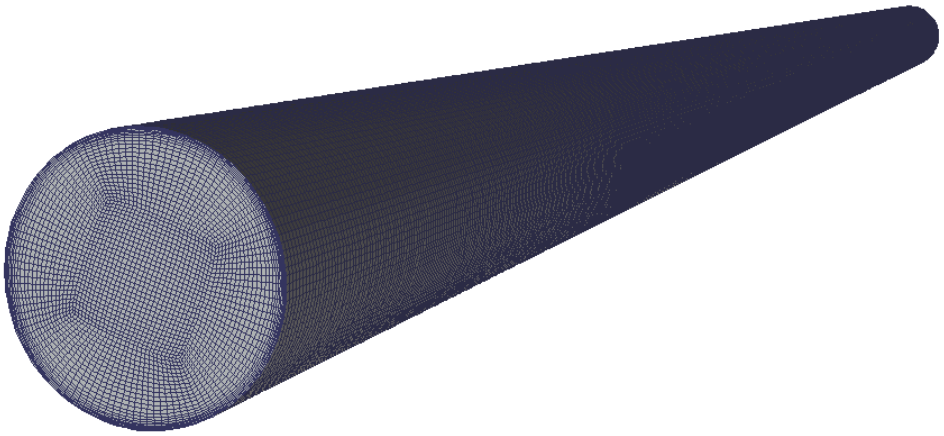

Figure 1: Grid structure for pipeline model.

4.2 Boundary Conditions

At the inlet, a velocity-inlet condition is selected. The velocities and concentrations of both phases are given specified values, with the particle phase having a slightly lower velocity than the liquid phases and the coarse particles being about 5% slower than fine particles. Turbulent intensity, turbulent viscosity ratio, and temperature are all set to their default values of 5%, 10, and 20 °C, respectively.

At the outlet, the pressure-outlet is selected, and the pressure is atmospheric. At the wall, the velocity of the liquid phase is set to zero (i.e., no-slip condition). The wall roughness is set to 0.02 mm, and the specularity coefficient (taken as 0.451) is selected for the shear condition of the solid phase. The particle condition follows the Johnson–Jackson model, and the restitution coefficient is set to 0.2.

4.3 Solving Process and Convergence Scheme

Commercial CFD software ANSYS Fluent 17.0 is used to solve the above continuum equations and boundary conditions. Convergence of the root-mean square residual is set to 10^{-5}. The solving method follows the phase-coupled SIMPLE function to ensure convergent, steady, and accurate results. The second-order upwind method is adopted to solve momentum equations, with the pressure relaxation factor set to 0.2, the momentum relaxation factor set to 0.3, and the volume fraction set to 0.4; other factors retain their default values.

5. Results and Discussion

To analyse a broad range of simulation results and experimental data in a limited space, some typical experimental conditions (Roco and Shook, 1983; Kaushal and Tomita, 2005; and Gillies *et al*., 2004) are simulated with ANSYS Fluent. They cover a wide range of particle diameters (0.09–0.44 mm), particle volume concentrations (9%–50%), slurry flow rates (2–5 m/s), and pipe diameters (51.5–495 mm). The simulation results are validated through comparison with the corresponding measured data for the steady-state particle concentration distribution and the particle and liquid velocity distributions in the pipes.

Three works by Kaushal and Tomita (2002, 2007) and Kaushal et al. (2005) give similar concentration profiles, but there are differences among a few cases for coarse (0.44 mm) particles at low flow velocities (Kaushal and Tomita, 2007). The values tabulated in Kaushal et al. (2005) are clearer and more convenient than the data given as figures in the other papers, and are thus selected here for comparison with the simulation results.

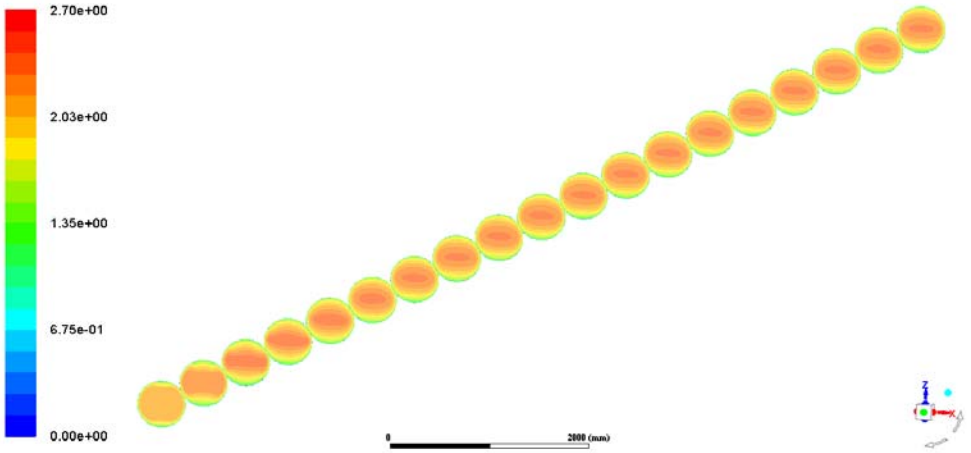

Figure 2: Contour plots for particle velocity taken at regularly spaced axial positions along the pipeline for the following conditions: D = 495 mm, d_p = 0.165 mm, C_{vf} = 27.3%, and v = 3.16 m/s

Figure 2 shows contour plots of liquid velocity distribution along the pipe cross-section at axial positions separated by 0.05L, where L is the length of the pipe simulation model. The simulation conditions are pipe diameter 495 mm, particle diameter d_p = 0.165 mm, solid volume concentration 27.3%, and slurry rate v = 3.16 m/s. The distributions differ significantly among the first six sections, but all the subsequent distributions appear nearly identical in each case. This shows that the model pipeline has sufficient length (60 times its diameter) and that the numerical slurry simulations provide fully developed results. The following simulation results are obtained near the outlet of the pipe model.

5.1 Solid Concentration Distribution

figure 3 shows a set of solid volume concentration contours on the left, and the curve on its centreline compared with experimental data on the right for 0.44 mm glass ball slurries flowing at a constant mixture velocity (4 m/s) in a 54.9 mm pipeline. The slurries differ in their solid volume concentrations: 20%, 30%, 40%, and 50%. The experimental data were initially reported by Kaushal et al. (2005). The simulation reasonably coincides with the experimental results, indicating that the model is suitable for simulating the particle concentration distribution for a wide range of solid concentrations.

As figure 3 shows, the solid volume concentration is asymmetric in the perpendicular direction. The asymmetry is reduced as the solid volume concentration increases at a given velocity, pipe diameter, and particle size because of increased particle–particle collisions. In figure 3A–C, the distances of the points of greatest particle concentration from the bottom of the pipe (about 0.1D) are simulated here for the first time: the results fit the experimental data well, indicating that the model can simulate the effect of wall lift force on the particle concentration distribution.

The point of greatest solid concentration in figure 3D is nearer to the pipe bottom than in the other images, because increasing the particle concentration leads to more particle–particle

and particle–wall collisions, which have a uniform effect far beyond the effect of the near-wall lift force. Increased interactions between particles increases the particle virtual mass force, and thus increases the ability of particles to remain suspended, leading to a more symmetric distribution in the pipe.

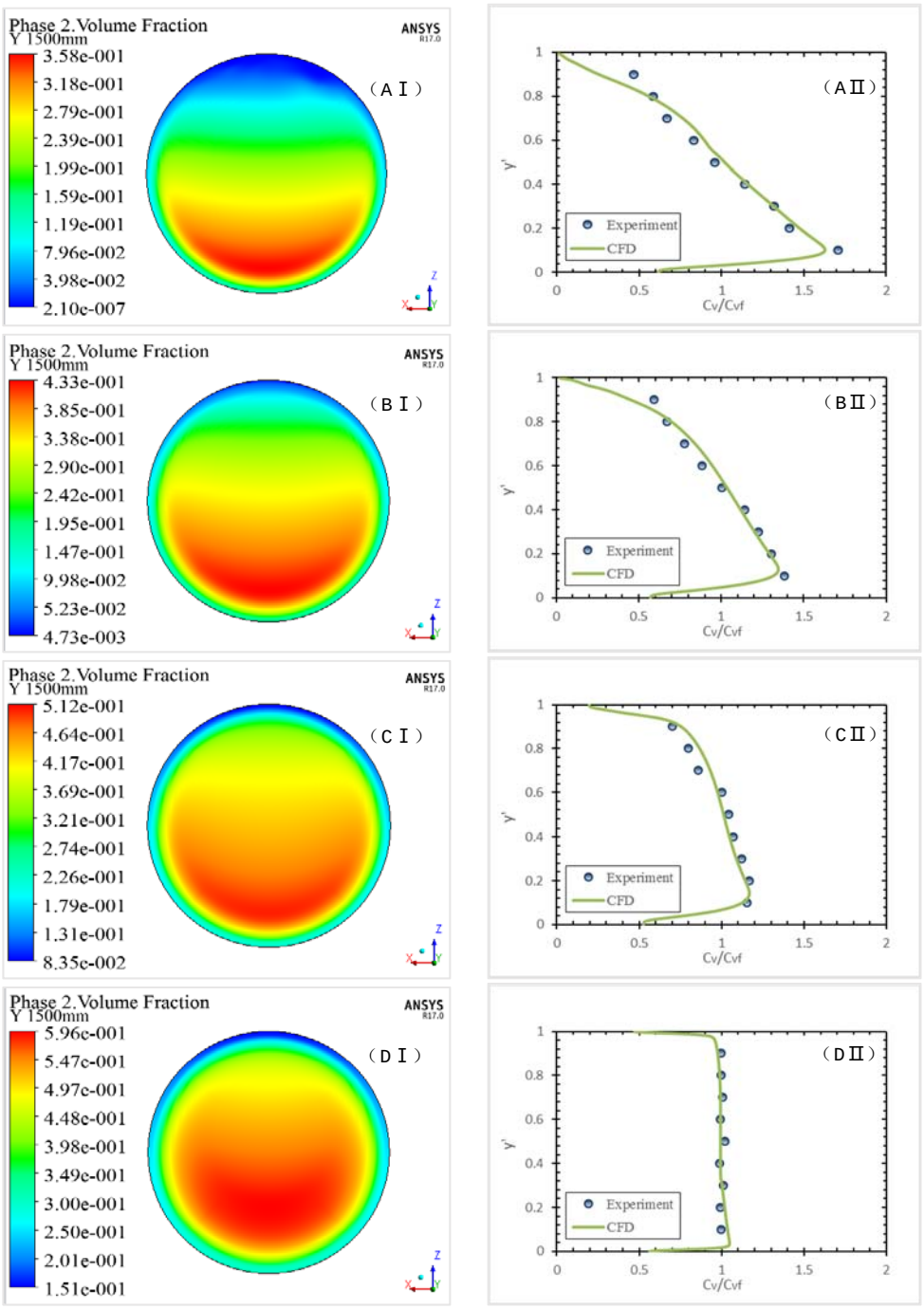

Figure 3: Particle volume concentration distribution for D = 54.9 mm, d_p = 0.44 mm, v = 4 m/s, and (A) C_{vf} = 20%, (B) C_{vf} = 30%, (C) C_{vf} = 40%, and (D) C_{vf} = 50%.

The ordinate axis, $y' = y/D$, is the dimensionless position along the pipe's vertical axis, where y is the distance from the pipe bottom, and the abscissa, C_v/C_{vf}, represents the relative solid volume concentration ratio on the vertical centreline of the pipe, where C_v is the local solid volume concentration and C_{vf} is the efflux solid volume concentration.

Figure 4 gives simulated solid concentration distributions for 0.125 mm glass balls in a

54.9 mm pipe with 30% solid concentration at different slurry velocities (2, 3, 4, and 5 m/s), and compares them with the experimental data of Kaushal et al. (2005). The results are nearly the same as the experimental data, demonstrating that the model can accurately simulate the concentration distribution of slurry pipeline transportation at a wide range of velocities.

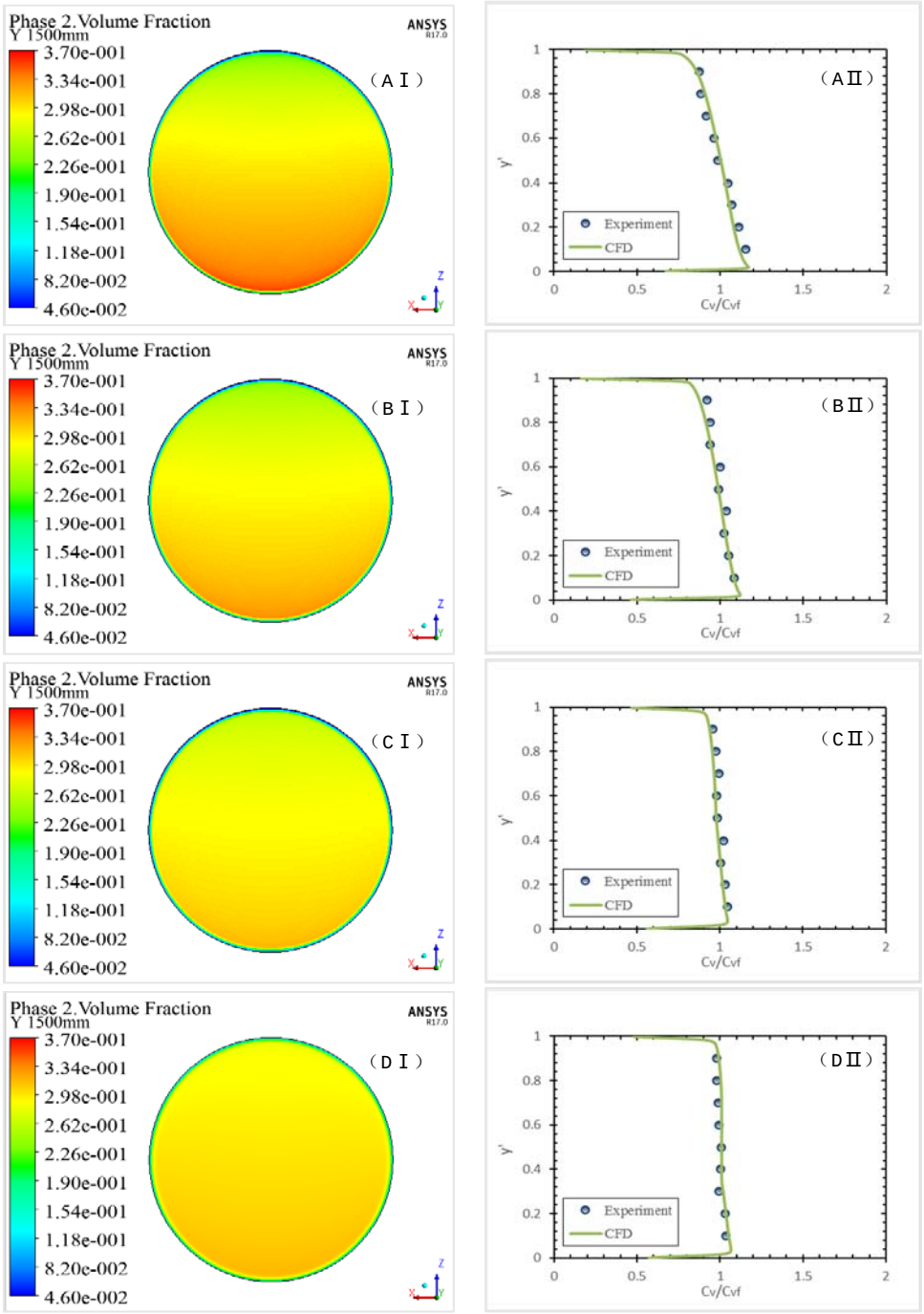

Figure 4: Particle volume concentration distributions for D = 54.9 mm, d_p = 0.125 mm, C_{vf} = 30%, and (A) v = 2 m/s, (B) v = 3 m/s, (C) v = 4 m/s, and (D) v = 5m/s.

The asymmetry of the slurry concentration curves is significantly reduced as the slurry velocity increases for the given conditions of constant concentration, pipe diameter, and particle size. This result arises because the particles are more easily suspended at increased velocity, which increases turbulence intensity and turbulent dissipation forces.

The maximum solid concentration is situated closer to the pipe bottom than in figure 3A–

C, and appears in the viscous sublayer. It remains close to the wall, and the particle concentrations then decrease rapidly because the particle size is less than the thickness of the viscous sublayer; thus, particles are not influenced by the near-wall lift force, and instead suffer from collisions with the wall.

The simulation results in figure 5 for four different particle sizes (0.09, 0.125, 0.27, and 0.44 mm) all agree well with experimental values by Kaushal et al. (2005) and Gillies *et al.* (2004).

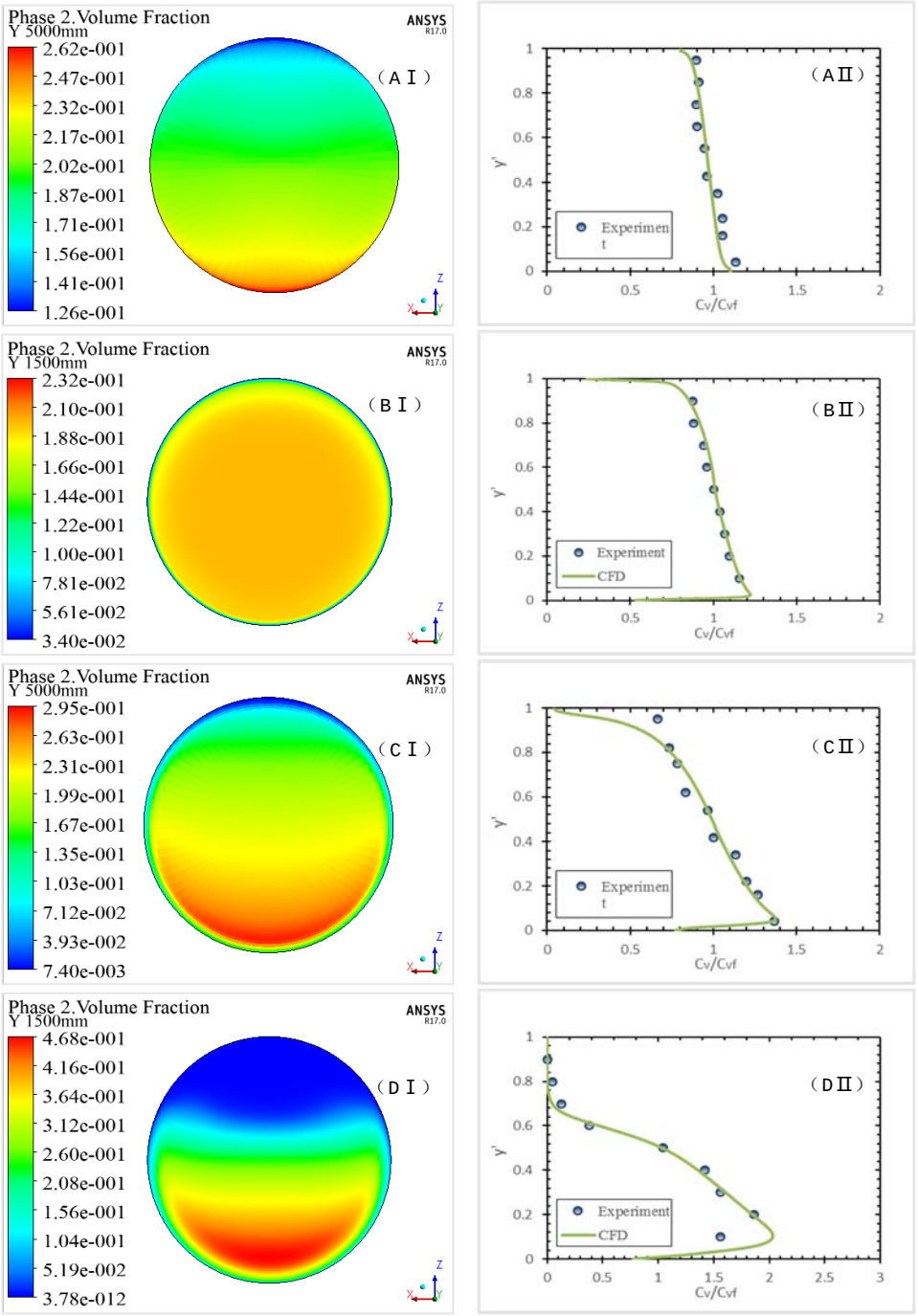

Figure 5: Particle volume concentration distributions for (A) d_p = 0.09 mm, D = 103 mm, C_{vf} = 19%, and v = 3 m/s; (B) d_p = 0.125 mm, D = 54.9 mm, C_{vf} = 20%, and v = 2 m/s; (C) d_p = 0.27 mm, D = 103 mm, C_{vf} = 30%, and v = 5.4 m/s; and (D) d_p = 0.44 mm, D = 54.9 mm, C_{vf} = 20%, and v = 2 m/s.

For similar flow conditions, the figure shows that as the particles become larger, their concentration distributions become more asymmetric in the pipe cross-section. The method of classifying slurry flow regimes given by Wasp et al. (1977) describes figure 5A (0.09 mm) as homogeneous, figure 5B and C (0.125 and 0.27 mm, respectively) as heterogeneous, and figure 5D (0.44 mm) as a sliding bed. Three different flow regimes and their changing trends with respect to particle size are thus simulated successfully.

Figure 5C and D appear similar to figure 3A–C, in terms of the location of the point of maximum solid volume concentration relative to the pipe bottom. Figure 5A and B are similar to figure 3D, with the reversal situated in the viscous sublayer.

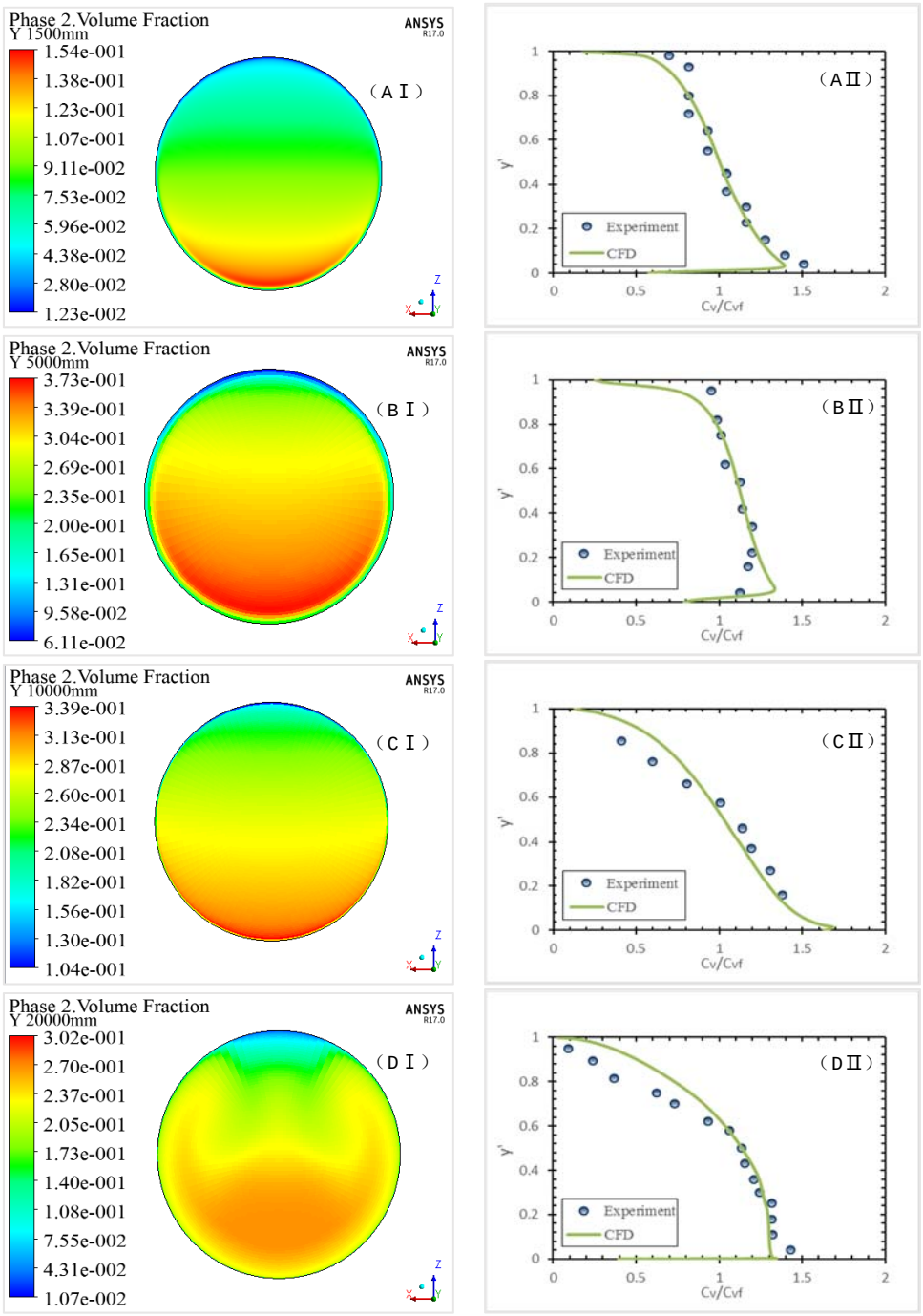

Figure 6: Particle volume concentration distribution for (A) D = 51.5 mm, d_p = 0.165 mm, C_{vf} = 9.18%, and v = 3.78 m/s; (B) D = 103 mm, d_p = 0.27 mm, C_{vf} = 40%, and v = 5.4 m/s;

(C) D = 263 mm, d_p = 0.165 mm, C_{vf} = 27%, and v = 2.9 m/s; and (D) D = 495 mm, d_p = 0.165 mm, C_{vf} = 27.3%, and v = 3.16 m/s.

The effects of pipe diameter on particle concentration distribution are modelled and compared with experimental data. The pipe models have diameters of 51.5, 103, 263, and 495 mm, corresponding to the experiments conducted by Roco & Shook (1983) and Gillies *et al*. (2004). The simulated results are consistent with the experimental results. Within a certain range, increasing the pipe diameter increases the asymmetry of the slurry concentration distribution on the vertical axis in the pipeline.

The clear difference between the simulation (which shows the greatest particle concentration situated at 0.1D above the pipe bottom) and the experiment (which shows it at 0.2D above the pipe bottom) in figures 4CII, 6DII, and 7BII may arise owing to the sparse concentration-measuring points near the pipe wall in the experiment.

5.2 Velocity Distribution

The solid velocity distribution is inextricably linked to its concentration distribution within the pipeline. A symmetric solid concentration distribution will have a symmetric velocity distribution. Figure 7 shows solid velocity distribution contours on the left and curves for the centreline compared with corresponding experimental data on the right. Figure 7A shows the simulated solid velocity distribution for 0.09 mm particles at 19% concentration in a 103 mm pipe with 3 m/s flow speed and the comparison with experimental data by Gillies *et al*. (2004). The distribution is relatively symmetric, and the point of maximum speed is slightly over the pipe centre.

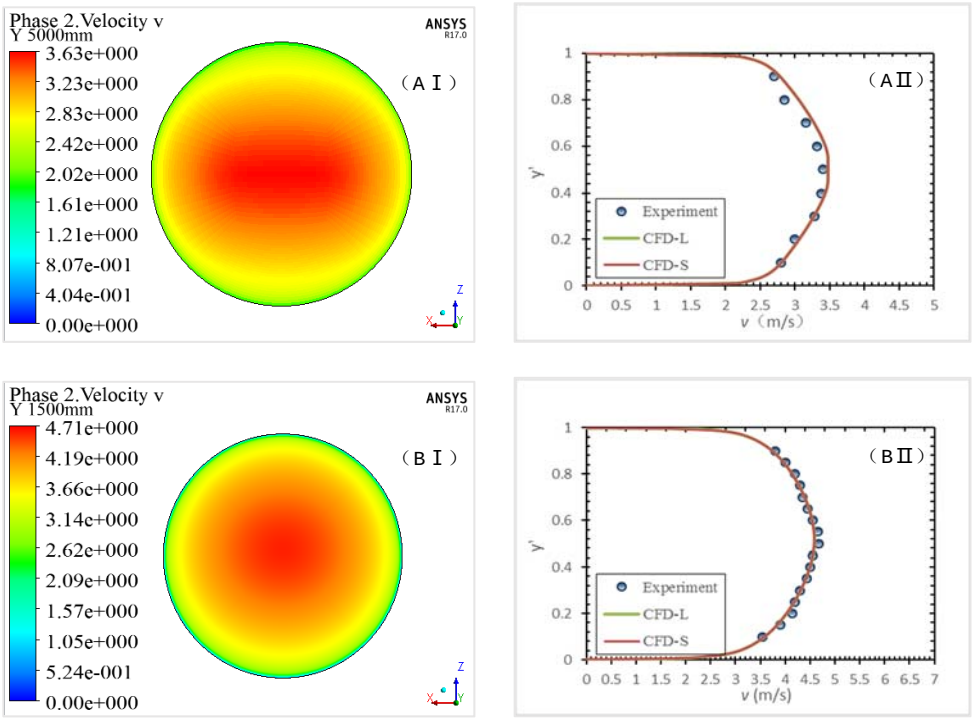

Figure 7: Solid velocity distribution for (A) D = 103 mm, d_p = 0.09 mm, C_{vf} = 19%, and v = 3m/s; and (B) D = 51.5 mm, d_p = 0.165 mm, C_{vf} = 9.18%, and v = 3.78 m/s.

Figure 7 also shows that particle velocity and liquid velocity are similar; thus, particle slip velocity of the slurry is very small. Figure 7B is the simulated solid velocity distribution for 0.165 mm particles at 9.18% concentration in a 51.5 mm pipe with 3.78 m/s mixture speed and

a comparison with experimental data by Roco & Shook (1983). The simulation agrees well with the experimental results, and its distribution is symmetric in the horizontal direction.

Figure 8 shows the simulated solid velocity distribution for 0.44 mm particles at different concentrations (20%, 30%, 40%, and 50%) in a 54.9 mm pipe at 4 m/s velocity (the solid volume concentration distribution is shown in figure 3). As the solid concentration increases, the point of maximum velocity gradually moves downward.

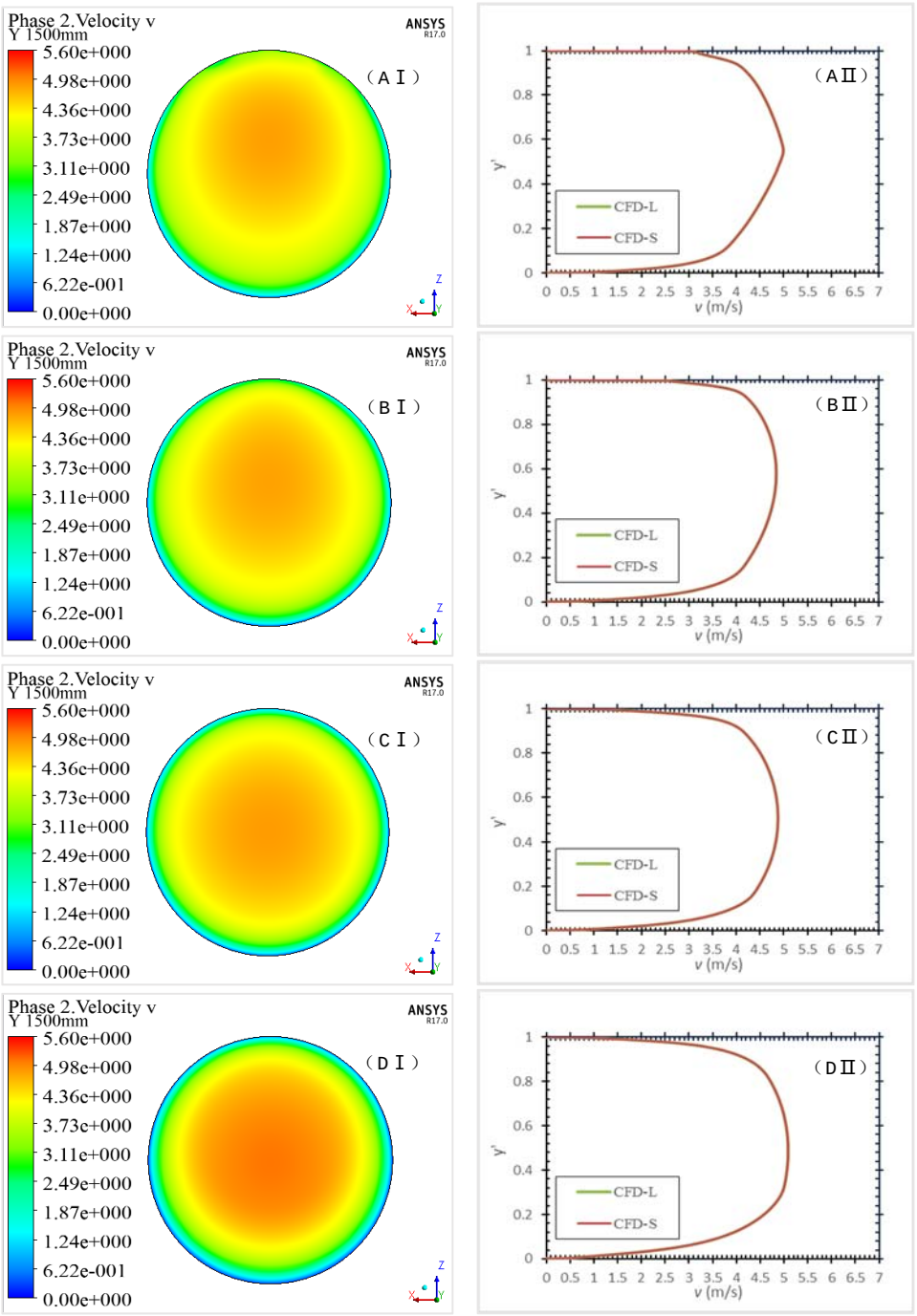

Figure 8: Solid velocity distribution for D = 54.9 mm, d_p = 0.44 mm, v = 4 m/s, and (A) C_{vf} = 20%, (B) C_{vf} = 30%, (C) C_{vf} = 40%, and (D) C_{vf} = 50%.

Figure 9 exhibits the simulated solid velocity distribution for 0.125 mm particles at 30% concentration in a 54.9 mm pipe with different velocities (2, 3, 4, and 5 m/s) (the solid volume

concentration distribution is shown in figure 4). The points of maximum velocity are close to the pipe centre.

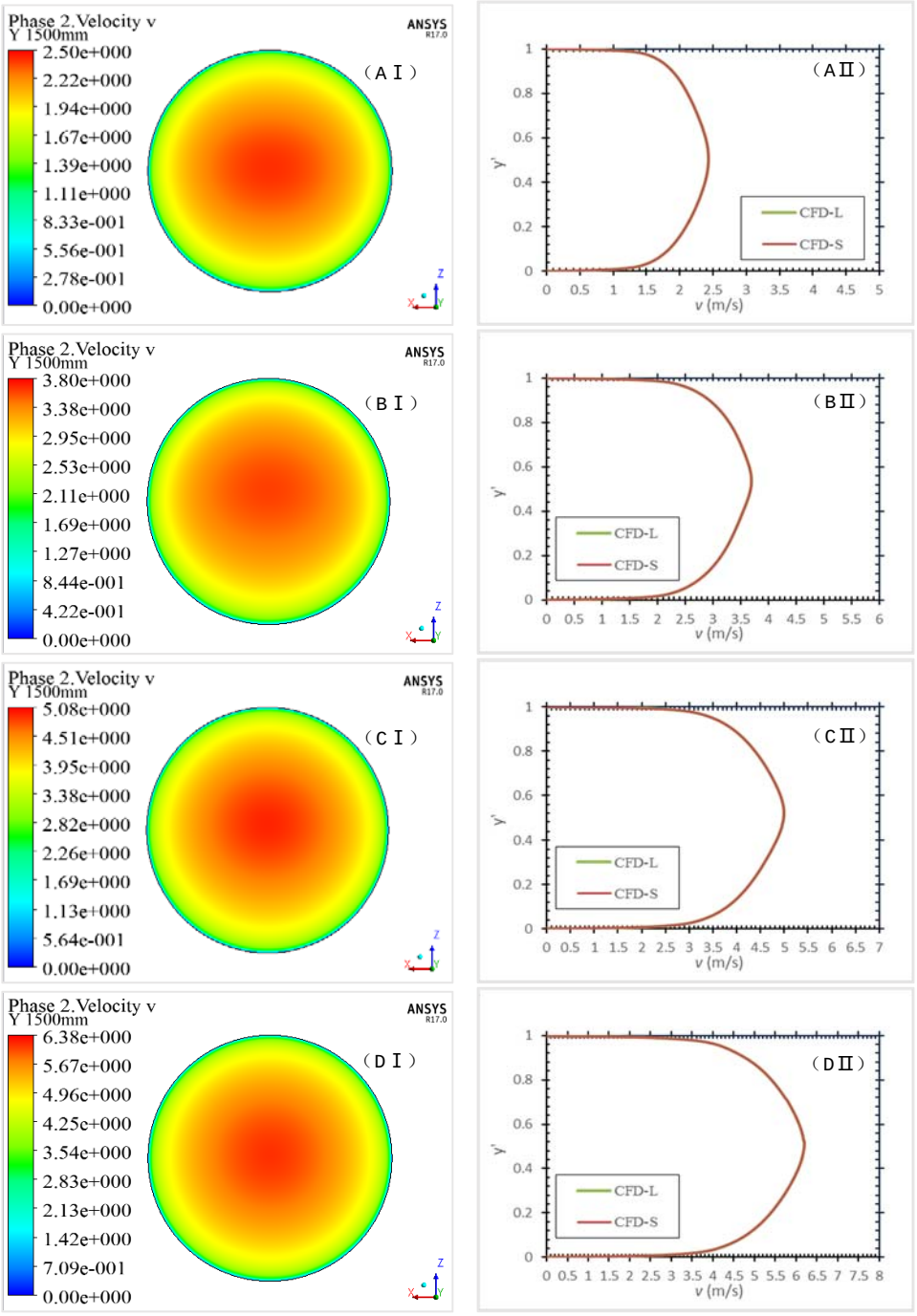

Figure 9: Solid velocity distribution for D = 54.9 mm, C_{vf} = 30%, d_p = 0.125 mm, and (A) v = 2 m/s, (B) v = 3 m/s, (C) v = 4 m/s, and (D) v = 5 m/s.

Comparing figures 9B and 10C (particle diameter 0.44 vs. 0.125 mm) shows that larger particles at the same velocity and concentration condition will be more asymmetrically distributed with a larger deviation of the point of maximum velocity from the pipe centre. This demonstrates that larger particles experience a greater influence of gravity, and the concentration increases at the bottom of the pipe, leading to a lower concentration and higher velocity at the top of the pipe.

6. Conclusions

A steady three-dimensional hydrodynamic model of slurry transport by pipeline is developed here based on the kinetic theory of granular flow. Parameters including solid volume concentration and velocity distributions are simulated for a wide range of typical working conditions, and compared with experimental data by Roco and Shook (1983), Kaushal and Tomita (2005), and Gillies *et al*. (2004). Over a wide range of situations, such as different particle sizes, particle volume concentrations, mixture velocities, and pipe diameters, the model's predictions agree well with the experimental data. The difference between the simulation results (which show maximum particle concentration situated at $0.1D$ above the pipe bottom) and the results of Kaushal and Tomita (2007) (who found the maximum particle concentration significantly above the pipe bottom) is well depicted in concentration profiles such as figures 4CII, 6DII and 7BII. Overall, the Eulerian multiphase model based on the kinetic theory of granular flow appears capable of predicting the solid concentration and velocity of slurry flows in pipelines. It also handles well the regime of slurry flow under a range of conditions, the effect of the near-wall lift force on the coarse particle concentration distribution, and the effect of particle–wall collisions on the solid concentration distribution near the wall.

The simulation shows that the solid volume concentration and velocity distributions in a pipe depend on factors such as the mixture velocity, pipe diameter, particle size, slurry concentration, and solid density. On the vertical centreline of the pipe, particle concentration and velocity distribution are asymmetric, with the degree of asymmetry depending on the pipe diameter, particle size, mixture velocity, and solid volume concentration. The asymmetry of the particle concentration distribution increases with increasing particles size, pipe diameter, and mixture velocity, and with decreasing solid concentration. Increasing the solid concentration gradually shifts the point of maximum velocity downward.

Most of the boundary conditions of the model are default values for the ANSYS Fluent program, thus simplifying the input data. The calculations are fast and easily convergence, making the present scheme a widely applicable and useful model.

Acknowledgments

This research work is supported by the National Natural Science Foundation of China (Grant No. 51779143) and State Key Laboratory of Ocean Engineering of Shanghai Jiao Tong University (Grant No. GKZD010071).

References

Durand R. (1952) *The Hydraulic Transportation of Coal and Other Materials in Pipes*, Collage of National Coal Board, London.

Doron, P., and Barnea, D. (1993) A three-layer model for solid-liquid flow in horizontal pipes, *International Journal of Multiphase Flow* **19**, 1029-1043.

Ekambara, K., Sanders, R. S., Nandakumar, K., and Masliyah, J. H. (2009) Hydrodynamic simulation of horizontal slurry pipeline flow using ANSYS-CFX, *Industrial and Engineering Chemistry Research* **48**, 8159-8171.

Gidaspow D., Bezburuah R., Ding J. (1992) Hydrodynamics of Circulating Fluidized Beds: Kinetic Theory Approach, *In Fluidization VII, Proceedings of the 7th Engineering Foundation Conference on Fluidization* 75–82.

Gillies, R. G., Shook, C. A., and Xu, J. (2004) Modelling heterogeneous slurry flows at high velocities, *Canadian Journal of Chemical Engineering* **82**, 1060-1065.

Karabelas, A. J. (1977) Vertical distribution of dilute suspensions in turbulent pipe flow, *Aiche Journal* **23**, 426–

434.
Kaushal, D. R., and Tomita, Y. (2002) Solids concentration profiles and pressure drop in pipeline flow of multisized particulate slurries, *International Journal of Multiphase Flow* **28**, 1697-1717.
Kaushal, D. R., Sato, K., Toyota, T., Funatsu, K., and Tomita, Y. (2005) Effect of particle size distribution on pressure drop and concentration profile in pipeline flow of highly concentrated slurry. *International Journal of Multiphase Flow* **31**, 809-823.
Kaushal, D. R., and Tomita, Y. (2007) Experimental investigation for near-wall lift of coarser particles in slurry pipeline using γ-ray densitometer, *Powder Technology* **172**, 177-187.
Kaushal, D. R., Thinglas, T., Tomita, Y., Kuchii, S., and Tsukamoto, H. (2012) Cfd modeling for pipeline flow of fine particles at high concentration, *International Journal of Multiphase Flow* **43**, 85-100.
Lahiri, S. K., and Ghanta, K. C. (2008) Prediction of pressure drop of slurry flow in pipeline by hybrid support vector regression and genetic algorithm model, *Chinese Journal of Chemical Engineering* **16**, 841-848.
Ling, J., Skudarnov, P. V., Lin, C. X., and Ebadian, M. A. (2003) Numerical investigations of liquid–solid slurry flows in a fully developed turbulent flow region, *International Journal of Heat and Fluid Flow* **24**, 389-398.
Lun, C. K. K., Savage, S. B., Jeffrey, D. J., and Chepurniy, N. (2006) Kinetic theories for granular flow: inelastic particles in couette flow and slightly inelastic particles in a general flow field, *Journal of Fluid Mechanics* **140**, 223-256.
Messa, G. V., Malin, M., and Malavasi, S. (2014) Numerical prediction of fully-suspended slurry flow in horizontal pipes, *Powder Technology* **256**, 61-70.
Messa, G. V., and Malavasi, S. (2015) Improvements in the numerical prediction of fully-suspended slurry flow in horizontal pipes, *Powder Technology* **270**, 358-367.
Miedema, S. A. (2015) A head loss model for slurry transport in the heterogeneous regime, *Ocean Engineering* **106**, 360-370.
Miedema, S. A. (2016a) A head loss model for homogeneous slurry transport for medium sized particles, *Journal of Hydrology and Hydromechanics* **63**, 1-12.
Miedema, S. A. (2016b) The heterogeneous to homogeneous transition for slurry flow in pipes, *Ocean Engineering* **123**, 422-431.
Miedema, S. A. (2017) *A new approach to determine the concentration distribution in slurry transport*, Dredging Summit and Expo. 2017, USA.
Miedema, S. A., and Ramsdell, R. C. (2015a) *Preview: Slurry Transport: Fundamentals, A Historical Overview and The Delft Head Loss and Limit Deposit Velocity Framework*, Delft University of Technology.
Miedema, S. A., and Ramsdell, R. C. (2015b) The limit deposit velocity model, a new approach, *Journal of Hydrology and Hydromechanics* **63**, 273-286.
Ogawa S., Umemura A., Oshima N. (1980) On the equations of fully fluidized granular materials, *Zeitschrift Für Angewandte Mathematik Und Physik Zamp* **31**, 483-493.
Roco, M. C., and Shook, C. A. (1983) Modeling of slurry flow: the effect of particle size, *Canadian Journal of Chemical Engineering* **61**, 494-503.
Schaeffer, D. G. (1987) Instability in the evolution equations describing incompressible granular flow, *Journal of Differential Equations* **66**, 19-50.
Turian, R. M., and Yuan, T. (1977) Flow of slurries in pipelines, *Aiche Journal* **23**, 232-243.
Wasp, E. J., Kenny, J. P., and Gandhi, R. L. (1977) *Solid-liquid flow slurry pipeline transportation*, Ser. Bulk Mater. Handl. USA.
Wilson, K. C., and Addie, G. R. (1997) Coarse-particle pipeline transport: effect of particle degradation on friction, *Powder Technology* **94**, 235-238.
Wilson, K. C., Clift, R., and Sellgren, A. (2002) Operating points for pipelines carrying concentrated heterogeneous slurries, *Powder Technology* **123**, 19-24.
Wilson, K. C., and Sellgren, A. (2003) Interaction of particles and near-wall lift in slurry pipelines, *Journal of Hydraulic Engineering* **129**, 73-76.
Wilson, K. C., Addie, G. R., Sellgren, A., and Clift, R. (2006) *Slurry transport using centrifugal pumps*, Springer Science+Business Medial Inc., USA.